Boundary-Layer-Tripping Studies of Compressible Dynamic Stall Flow

M. S. Chandrasekhara*
U.S. Naval Postgraduate School, Monterey, California 93943
M. C. Wilder†
MCAT Institute, San Jose, California 95127
and
L. W. Carr‡
U.S. Army Aeroflightdynamics Directorate, Moffett Field, California 94035-1000

The challenging task of properly tripping the boundary layer of a leading-edge-stalling airfoil experiencing compressible dynamic stall at Reynolds numbers between 3.6×10^5 and 8.1×10^5 has been addressed. Real-time interferometry data of the flow over an oscillating airfoil have been obtained at freestream Mach numbers of 0.3 and 0.45. The airfoil was tripped by separately placing five different trips of varying lengths near the leading edge. The trip heights ranged from 40 to 175 μm. The resulting flow and airfoil performance were evaluated using the criteria of elimination of the laminar separation bubble that otherwise forms, delay of dynamic stall onset to higher angles of attack, and production of consistently higher suction peaks. Quantitative analysis of the interferograms showed that the laminar separation bubble was still present with the smallest trip and premature dynamic stall occurred with the largest trip. The right trip was determined to be a distributed roughness element extending from 0.5 to 3% chord. Its height was found to compare reasonably with the airfoil boundary-layer thickness at the dynamic stall vortex formation angle of attack, at a location slightly upstream of the vortex origin in the adverse pressure gradient region.

Nomenclature

C_p = pressure coefficient
$C_{p_{min}}$ = peak suction pressure coefficient
c = airfoil chord
f = frequency of oscillation, Hz
k = reduced frequency, $\pi f c / U_\infty$
M = freestream Mach number
Re = Reynolds number based on chord
U_∞ = freestream velocity
x, y = chordwise and vertical distance
α = angle of attack
α_m = amplitude of oscillation
α_0 = mean angle of attack
ω = circular frequency, rad/s

I. Introduction

LIFT enhancement by unsteady airfoil motion through the production of coherent vorticity is a problem of both fundamental and practical interest. The potential benefits of dynamically delaying stall of an airfoil offers possibilities for expanding the flight envelope of full-scale aircraft systems. However, the onset of compressibility effects at even low forward flight speeds complicates the problem of dynamic stall. In addition to introducing some basic fluid physics issues, compressibility promotes stall. The various factors affecting the problem are such that hitherto only wind-tunnel experiments have been conducted and flight tests are extremely expensive and difficult to perform. With the exception of McCroskey et al.[1] and Lorber and Carta,[2] the available experiments have been at low Reynolds numbers. The ongoing dynamic stall research[3,4] is at Reynolds numbers ranging from 3.6×10^5 to 8.1×10^5. This has shown that dynamic stall of an oscillating (or a transiently pitching) airfoil originates from the failure of the laminar separated flow to reattach as the angle of attack increases, resulting in the formation of the dynamic stall vortex from the bursting of a separation bubble. Since the separation bubble is a consequence of transition of the laminar separated shear layer, it can be concluded that transition physics plays a major role in the dynamic stall process. The ability of a boundary layer to overcome the strong adverse pressure gradient that follows the airfoil suction peak or of a layer of coherent vorticity to remain such without coalescing into vortical structures (flow separation) can be expected to depend on the state of turbulence in this transitional shear layer. Also the time scales of viscous (vorticity) diffusion and unsteadiness play an important role in the process. Additional complexity is introduced by the ever-changing transition behavior such as reduction of transition length with increasing pressure gradient[5] (as the airfoil pitches to a higher angle of attack). Thus, it is desirable to remove the effects of transition by predetermining the transition point and fixing it so that the effects of compressibility due to the large local fluid velocities around the leading edge can be clearly isolated.

Traditionally, fluid dynamicists have tripped the boundary layer in the hope of achieving Reynolds number similarity and removing transition effects as a parameter in low-Reynolds-number studies. Jones and Williams,[6] after an extensive study of NACA 0012 and RAF 34 airfoils, concluded that at low speeds these airfoils could be tripped in the same way pipe flows are tripped. However, the stall behavior of a NACA 0012 airfoil changes from that of trailing-edge stall to leading-edge stall when compressibility effects set in at $M = 0.3$ making this approach not applicable. The challenge

*Associate Director and Research Professor, Department of Aeronautics and Astronautics, Navy—NASA Joint Institute of Aeronautics; mailing address MS-260-1, NASA Ames Research Center, Moffett Field, CA 94035-1000. Associate Fellow AIAA.
†Research Scientist, Navy—NASA Joint Institute of Aeronautics.
‡Research Scientist and Group Leader, Unsteady Viscous Flows, U.S. Army Aviation Troop Command, U.S. Army Aviation Research, Development, and Engineering Center, NASA Ames Research Center. Member AIAA.

is, of course, finding the right trip that works satisfactorily over the range of flow conditions of interest. Much of the prior recommendations about the right trips have been based on estimates of the drag coefficient and its behavior.[7,8] Generally, a trip size (height and length) that produces no significant additional drag, but which would still produce a fully developed turbulent boundary layer over the flow surface, is chosen. In a way, this approach assumes that the boundary layer attains equilibrium some distance downstream of the trip. However, the choice is not clear when leading-edge stalling airfoils, or flows in which stall originates near the trip location, are to be investigated. This is especially the case for the dynamic stall flow, which is often a leading-edge type stall occurring just downstream of the suction peak. Furthermore, a stall vortex develops rapidly over a small angle of attack range with strength depending upon the degree of unsteadiness; thus, the flow is never in equilibrium. In addition, transition significantly affects the intricate details of the dynamic stall process such as the peak suction development, the maximum adverse pressure gradient before vortex formation, the type of shock/boundary-layer interaction in the locally supersonic flow, etc. Preston[9] recommends that any device used for achieving transition close to the leading edge must be considered in terms of both its drag-producing and disturbance-producing abilities. This is because the effectiveness of the device depends upon the momentum thickness Reynolds number in the laminar boundary layer at the point of tripping. Since there is a minimum value[9] for the momentum thickness Reynolds number for a turbulent boundary layer, the effectiveness of a trip could change with changes in the momentum thickness Reynolds number due to variations in unsteadiness and airfoil angle of attack. Hence, it is not surprising that there is no satisfactory tripping technique to be found in the literature for unsteady flow.

This paper attempts to quantify the dynamic stall process with five different trips and recommends a trip that seems to be the most appropriate for the problem. Experimental results of the flow over a steady and an oscillating NACA 0012 airfoil, obtained using the real-time technique of point diffraction interferometry (PDI), are presented. The flow Mach number was 0.3 and 0.45; the reduced frequency, $k = \pi f c / U_\infty$, was 0.0 (steady), 0.05, and 0.1. Measurements of both local and global pressures (density) have been obtained for each trip over the airfoil. The data for the tripped flows have been compared with each other and with that for the untripped airfoil flow. The results are presented in terms of the flowfield description as interpreted from the interferograms, the pressure distributions including the variation of the peak suction pressure coefficient, and the pressure gradients. It is hoped that the experimental data produced by this study will serve as benchmark data and help computationalists develop codes incorporating correct dynamic stall physics.

II. Description of the Experiment

A. Facility

The experiments were conducted in the NASA Ames Compressible Dynamic Stall Facility (CDSF). The CDSF is an indraft wind tunnel with a 35 × 25 cm test section. The tunnel is connected to a 240,000 cubic ft/min, 9000-hp evacuation compressor that allows continuous running at all flow speeds. The oscillatory motion is produced by a drive system located on top of the test section. It is connected to the test section windows by connecting rods on both sides. The windows are mounted in bearings and the airfoil is supported between the windows by small pins providing optical access down to the airfoil surface. A sinusoidal motion of the windows results in a sinusoidal variation of the airfoil angle of attack. Triangular registration markers are placed on the windows such that the line joining the vertical sides of the markers above and below the airfoil surface passes through the 25% chord point.

The drive is equipped with an incremental position encoder that provides instantaneous angle of attack and frequency/phase angle of oscillation of the airfoil. An absolute position encoder indicates the mean angle of attack that can be set from 0 to 15 deg. The amplitude of oscillation ranges from 2 to 10 deg and the oscillation frequency from 0 to 100 Hz. The nondimensional flow parameters that can be obtained in the CDSF correspond to those of a helicopter in forward flight and the Reynolds number corresponds to that of a one-seventh scale model rotor, whose test results are directly applicable to a helicopter rotor. Additional details of the system can be found in Carr and Chandrasekhara.[10]

The flow uniformity in the tunnel is ±0.25% at 58 m/s, and the turbulence intensity is 0.083% with a bandwidth of 50–50,000 Hz.[11]

B. Description of the Trips

A review of literature[7,8] was conducted to obtain the first estimate of the required trip size. The leading-edge-stalling NACA 0012 airfoil flow bears considerable qualitative similarity to the flow over a circular cylinder. Therefore, it was decided to use a roughness strip as the tripping device following the recommendations of Nakamura and Tomonari.[7] A formula given in Ref. 8 was used to arrive at the minimum size of the trip for the boundary layer. As reported in Wider et al.,[12] this formula indicated a grit size diameter of 56–89 μm (0.0022–0.0035 in.) for $0.2 \leq M \leq 0.3$. Boundary-layer transition trips were formed by bonding three-dimensional roughness elements in a spanwise strip of height 170 μm along the surface of the airfoil. Wind-tunnel tests were performed with this trip in place. The results indicated premature stall,[12] attributable to the large trip height resulting from the fabrication process used. Thus, it became necessary to conduct a systematic investigation and perform tests with different trip heights to identify a trip that yielded acceptable results. A total of five trip configurations having the following characteristics were tested.

Trip 1: 74–89-μm-diameter carborundum grains (number 220 polishing grit) were bonded to the airfoil surface using a water-soluble adhesive (Polaroid print-coating material). The strip was located on the upper surface for $0.005 \leq x/c \leq 0.03$. The average height of the trip was 170 μm.

Trip 2: A repeat of trip number 1 using a spray-on enamel lacquer adhesive. The average height of this trip was 100 μm. The lacquer was used for all subsequent trips.

Trip 3: Made of the same materials as trip number 2, this strip covered the entire leading edge starting on the lower surface at $x/c = 0.05$ (near the mean stagnation point) and extending to the upper surface at $x/c = 0.03$. The average height was approximately 130 μm.

Trip 4: A smaller grit material, 22–36 μm aluminum oxide particles, was used for trips 4 and 5. Trip number 4 was located on the upper surface, $0.005 \leq x/c \leq 0.03$, like trips 1 and 2. The trip was estimated to be no higher than 43 μm.

Trip 5: The last trip extended from $x/c = 0.05$ on the lower surface around the leading edge to $x/c = 0.05$ on the upper surface. The trip height was approximately 40 μm.

The trip heights were estimated from digitized airfoil images taken under no-flow conditions by magnifying and scaling the images on an IRIS workstation. The uncertainty in the estimated trip heights is ±10 μm. Since the trip height in relation to the local boundary-layer thickness is an important factor, it was necessary to determine the latter. The boundary-layer thickness was estimated from the interferograms by assuming that the layer is fully represented by the height of the fringe closest to the airfoil near the trip location. However, in view of the strong dependency of the boundary-layer thickness on Reynolds number, Mach number, angle of attack, reduced frequency, and location over the airfoil, only rough estimates could be generated. For example, at an angle of attack of 10 deg, the boundary-layer thickness was determined to be about 60 μm close to the suction peak and about 100 μm slightly upstream of the origin of the laminar separation bubble ($x/c \approx 0.01$).

C. PDI Technique

PDI is a real-time interferometry technique that uses fluid density changes to produce flow interferograms. Figure 1 shows the schematic of the optical arrangement used. It is similar to a standard schlieren system, with the light source replaced by a pulsed Nd-YAG laser and a predeveloped photographic plate located at the knife edge plane. The principle has been detailed in Ref. 13 and is briefly described here. A pinhole was created (burned) in situ in the photographic plate by increasing the laser energy, with no flow in the wind tunnel. This served as the point diffraction source for
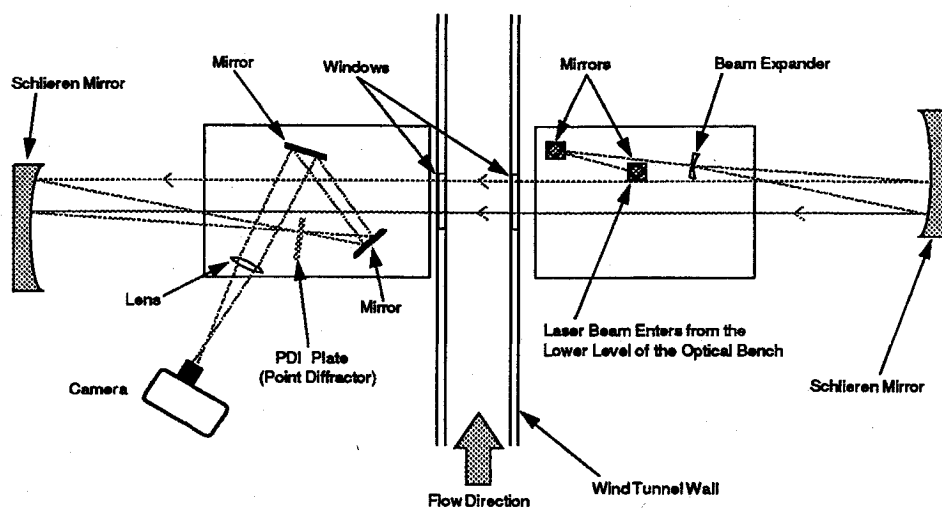
Fig. 1　Schematic of the PDI optical arrangement.

producing spherical reference waves. When the flow was turned on, the cylinder of light passing through the test section experienced phase shifts depending upon the local flow conditions and the beam exiting the tunnel window focused to a slightly larger spot around the pinhole. Since light passing through the pinhole loses all of the phase information introduced by the flow due to the spatial filtering characteristics of the pinhole, a reference wave is created in the light beam passing beyond the pinhole. This reference wave subsequently interfered with light that was transmitted around the pinhole through the photographic plate, producing interference fringes in real time at the image plane of the optics system. In operation, the laser was triggered stroboscopically, in a manner similar to that used in schlieren studies. No delays could be detected between the events of triggering the laser and the resulting laser light flash even at the highest frequency of oscillation tested.

D.　Image Processing

The analysis of the interferograms was conducted with software developed in house for the purpose. The surface pressure distributions were obtained by determining the fringe intersections with the airfoil contour. The pressure field was obtained by mapping the fringes in the images. For both, digitized PDI images are required as input. Using isentropic flow relations, the fringe numbers and, hence, the fluid densities were converted to pressure coefficients. This assumption was used even for the boundary layer and through the dynamic stall vortex. However, it is believed that substantial errors are not introduced in the pressure field, since the entropy change is generally small, until deep dynamic stall occurs.

E.　Experimental Conditions

The experiments were conducted on a 7.62-cm-chord NACA 0012 airfoil. Results will be presented here for flow Mach numbers of 0.3 and 0.45. The corresponding Reynolds numbers were 5.4×10^5 and 8.1×10^5, respectively. In addition to steady flow data, unsteady flow data was obtained for $k = 0.05$ and 0.1 at $M = 0.3$ and for $k = 0.05$ at $M = 0.45$, for the untripped airfoil and for each of the tripped airfoils. The airfoil was oscillated about the 25% chord point, with its angle of attack varying as $\alpha = 10$ deg–10 deg sin ωt. A large number of interferograms were obtained at close intervals depending on the event being imaged. The interval was less than 0.1 deg (one encoder count) during initiation of the dynamic stall process.

F.　Experimental Uncertainties

The estimated uncertainties are as follows: Mach number, ± 0.005; angle of attack, 0.05 deg; reduced frequency, 0.005; $C_{p_{min}}$, ± 0.075 at $M = 0.3$ and ± 0.0375 at $M = 0.45$; and $[dC_p/d(x/c)]$, ± 15.

The uncertainty in C_p depends on the fringe number under consideration and is estimated to be one fringe for the flow in general

with about three fringes possibly undetectable near the suction peak.

III.　Results and Discussion

A large number of interferograms were obtained and analyzed. Only typical photographic images will be presented here; the results from the others have been included in graphs to be discussed in this section.

A.　Qualitative Flow Description

Figure 2 presents the PDI images at $\alpha = 10$ deg for the untripped airfoil and for trips 3, 4, and 5 for $M = 0.3$ and $k = 0.05$. The fringes seen are constant density contours. In all images, the stagnation point is enveloped by the fringe closing around itself near the leading edge on the lower surface. Near the leading edge, the rapid fluid acceleration causes a large density change, resulting in a large number of fringes, which then radiate outward. For the untripped case, Fig. 2a, some of these fringes become parallel to the upper surface immediately after the suction peak and then turn sharply towards the surface. Based on past studies[14] this fringe pattern indicates a laminar separation bubble. The fringes turn sharply again as they merge with the redeveloping boundary layer. In Figs. 2b and 2c, the aforementioned pattern is not seen; the conclusion is that no laminar separation bubble is present in these cases since the fringes merge gradually with the boundary layer. The pressure distributions corresponding to these images (to be discussed in Sec. III.B.3) show a plateau for the untripped case that is absent in those for trip 4, pointing to the absence of the bubble with trip 4. Elimination of the bubble confirms the functional effectiveness of trip 4. Fringes in Fig. 2d for trip 5 exhibit a pattern indicative of the presence of the bubble, although its length is clearly smaller compared with that seen in Fig. 2a.

Figure 3 shows the flow details at $\alpha = 14$ deg when the dynamic stall process is in its beginning stages for the tripped cases. (The triangular markers seen on the images provide a reference length scale to map the airfoil during image processing, see Sec. II.A.) For the case of the untripped flow (Fig. 3a), the dynamic stall process is already under way by this angle since the center of the dynamic stall vortex has moved to about 25% chord location (its downstream edge has reached the 50% chord location). On the other hand, in the case of trip 3 (Fig. 3b), the process appears to have only just been initiated. This is indicated by the appearance of vertical fringes near the leading edge.[15] The outer fringes take a sharp turn towards the trailing edge at around $x/c = 0.35$, but the inner fringes are normal to the surface close to the leading edge. Beyond $x/c = 0.05$ they are oriented towards the trailing edge in general. For the case of trip 4 (Fig. 3c), this turn in the outer fringes occurs at $x/c = 0.25$ and the inner fringes still show a gradual variation in their orientation. A close examination reveals that only a few fringes have become vertical, and hence the dynamic stall process is still beginning. Trip 5 (Fig. 3d) shows an evolution that is midway between that of trips 3 and 4.
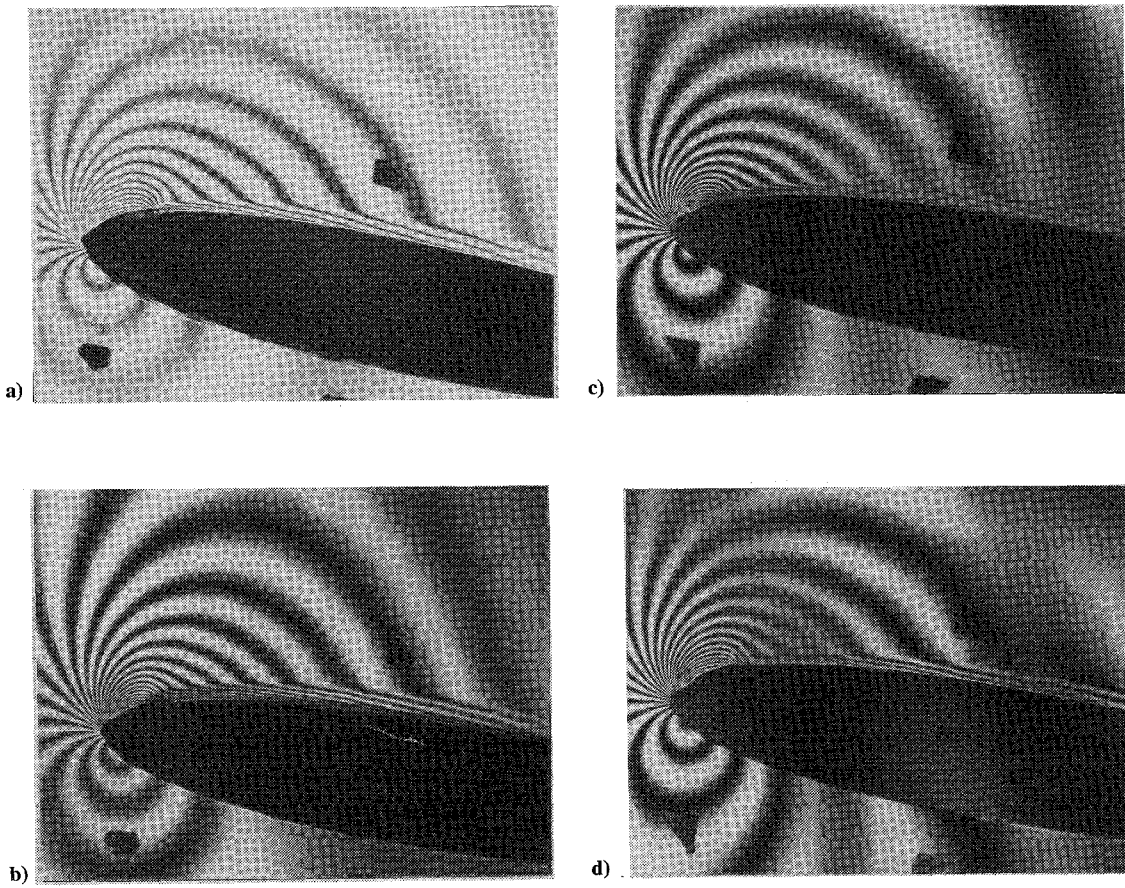
Fig. 2   PDI images of untripped and tripped flows for $M = 0.3$, $k = 0.05$, and $\alpha = 10.0$ deg: a) untripped, b) trip 3, c) trip 4, and d) trip 5.
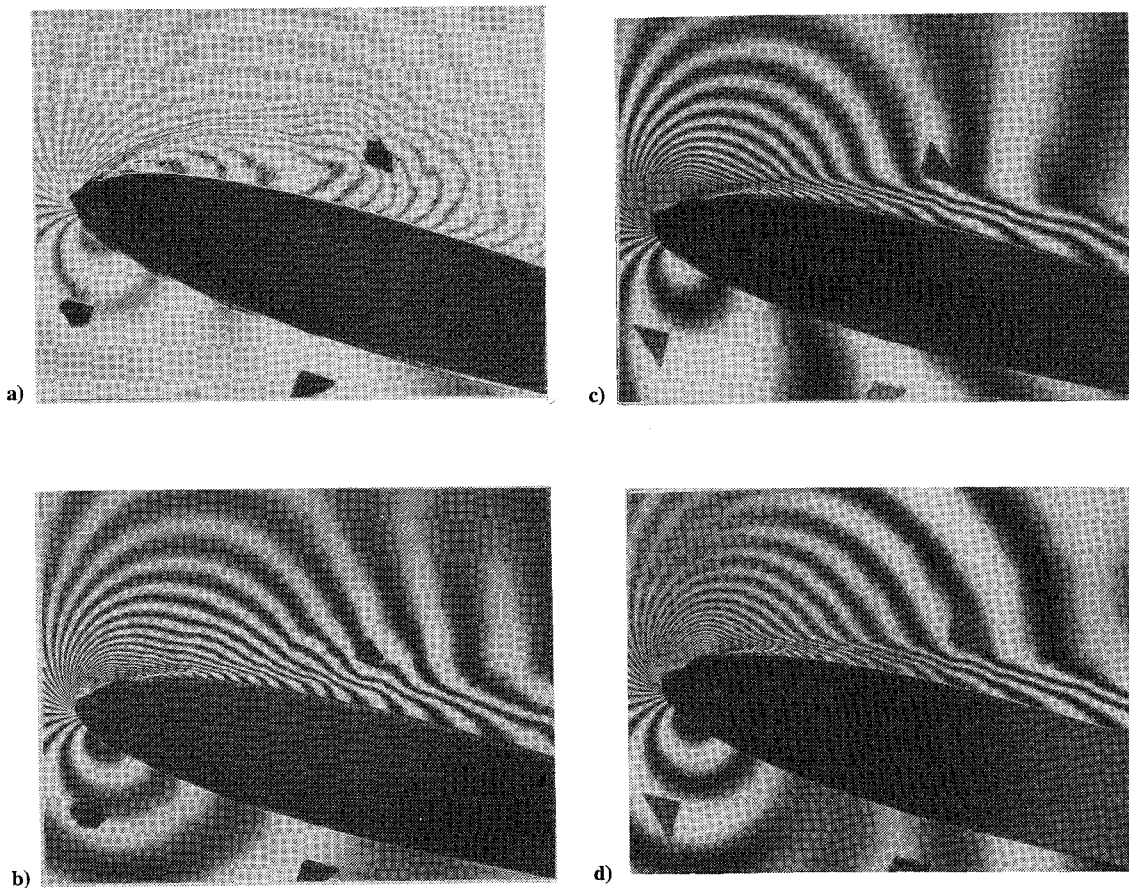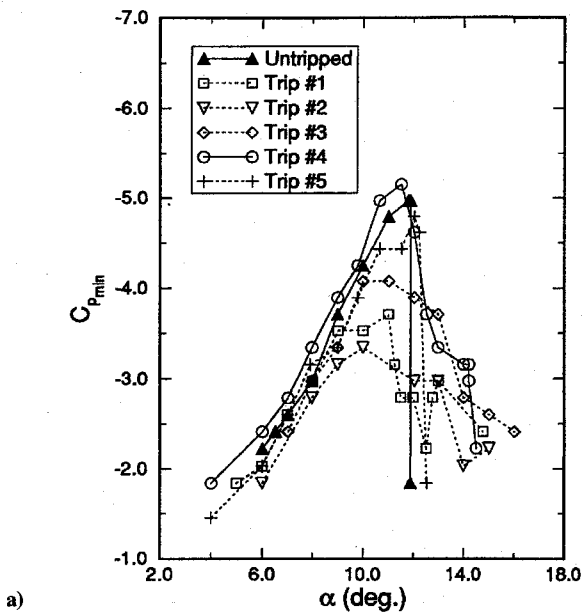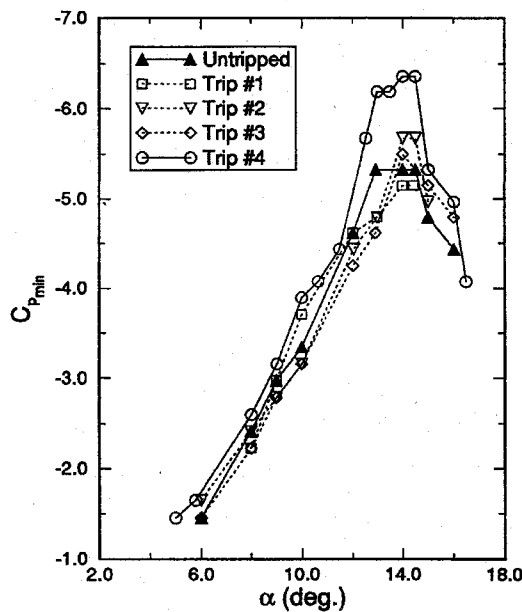
Fig. 3   PDI images of untripped and tripped flows for $M = 0.3$, $k = 0.05$, and $\alpha = 13.99$ deg: a) untripped, b) trip 3, c) trip 4, and d) trip 5.

a)

b)

Fig. 4   Effect of tripping on the development of peak suction pressure coefficient; $M = 0.3$: a) $k = 0$ and b) $k = 0.1$.
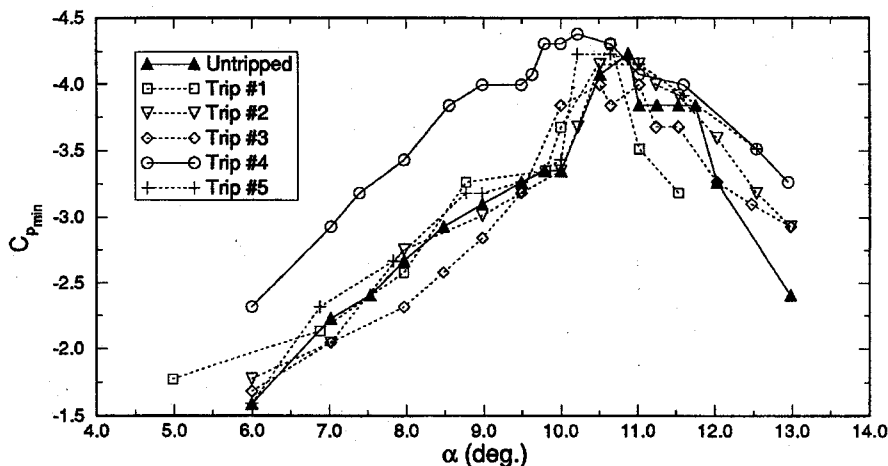
B. Quantitative Flow Analysis

1. Comparison of Trip Performance

Figure 4a shows the airfoil peak suction pressure coefficient, plotted vs angle of attack, for the untripped airfoil and for trips 1, 2, 3, 4, and 5 in steady flow at $M = 0.3$. The untripped airfoil experiences leading-edge stall at $\alpha = 12$ deg as seen by the abrupt loss of leading-edge suction. With trip 1 in place, the airfoil develops consistently lower peak suction levels than when it is untripped. Also, the static stall angle of 11 deg is lower than the static stall angle of 12 deg for the untripped case. Thus, it is clear that trip 1 actually degrades the airfoil performance. The airfoil with trip 2 or trip 3 is also unable to develop the high levels of suction expected of a turbulent flow. Also, the peak suction level reaches a maximum value at $\alpha = 10$ deg and then falls gradually, indicating a very different type of stall, resembling that of a trailing-edge-stalling airfoil. This radical change in steady stall behavior demonstrates the sensitivity of the flow to the design of the tripping mechanism and points to the need for properly tripping the airfoil. The performance of the airfoil with trip 4, as measured by the production of higher suction peaks as a function of angle of attack, is distinctly superior relative to its untripped counterpart. Eventually, at $\alpha = 11.6$ deg, the highest value of $C_p = -5.2$ is reached, (slightly higher than the $C_{p_{min}} = -4.9$ obtained with the untripped airfoil) before the airfoil experiences abrupt leading-edge stall. The performance for trip 5 is worse than that of the untripped airfoil. Since a separation bubble still forms in this case, trip 5 is deemed not to have worked for the purpose. It is very interesting to note that this trip does not suppress the bubble, even though it was in place starting at the stagnation point. It appears from this figure that the flow over the airfoil with trip 4 experiences a slightly greater acceleration, more like what is expected of turbulent flow. Still the increase is marginal and it is difficult to draw definitive conclusions from the information presented in this plot alone.

Figure 4b provides similar information when the airfoil is oscillating at a reduced frequency of 0.1 for the airfoil with no trip and with trips 1, 2, 3, and 4. It is clear that with trip 4 the airfoil develops suction peaks that are much higher than for the other cases plotted. Trips 1, 2, and 3 cause the airfoil performance to be generally worse than without a trip. In the case of trip 4, the $C_{p_{min}}$ value continues to increase to about -6.3 at $\alpha = 13.5$ deg when the dynamic stall process begins. The suction peak remains at this level during the process of dynamic stall vortex formation[15] and drops only after the vortex begins to convect. For the untripped airfoil, the vortex forms at a slightly lower angle of attack (approximately 12.5 deg) and at a much lower suction peak of -5.4. Thus, a delay of stall and an increase of suction level are both achieved with trip 4 on the airfoil, leading to the conclusion that the boundary layer was successfully tripped.

Results for $M = 0.45$ and $k = 0.05$ for all cases are presented in Fig. 5. For this higher Mach number case, trip 1 was not as detrimental as it was for $M = 0.3$. This is because the height of the trip relative to the local boundary-layer thickness is smaller in this case, and hence the momentum loss due to its presence is reduced.

Fig. 5   Effect of tripping on the development of peak suction pressure coefficient; $M = 0.45$ and $k = 0.05$.

However, the suction developed is still not acceptable. Results for trips 1, 2, and 3 are all within the experimental scatter from the untripped case for most part. In comparison, it is clear that trip 4 is successful even at $M = 0.45$. The unsteady flow peak suction pressures plotted in Fig. 5 for a reduced frequency of 0.05 show that the airfoil with trip 4 consistently produced higher levels of suction than the untripped or trip 5 airfoils. Beyond an angle of attack of 8.5 deg trip 5 showed a small bubble. It is further interesting to note that all six flows attained values of $C_{p_{min}}$ larger than the critical C_p value of -2.7 for $M = 0.45$; thus, the flow was locally supersonic in all six cases. But the highest $C_{p_{min}}$ value was found with trip 4, and thus the supersonic velocities were the largest in this case. Even so, a slight delay of stall was observed.

2. Airfoil Pressure Distributions

The pressure distributions over the airfoil for $M = 0.3$ and $k = 0.05$, obtained by image processing of the interferograms, are plotted in Fig. 6a, where the surface C_p for untripped flow and for trip 4 at $\alpha = 10.65$ deg are shown. The plateau seen for the untripped flow is caused by the presence of the bubble. The distribution for trip
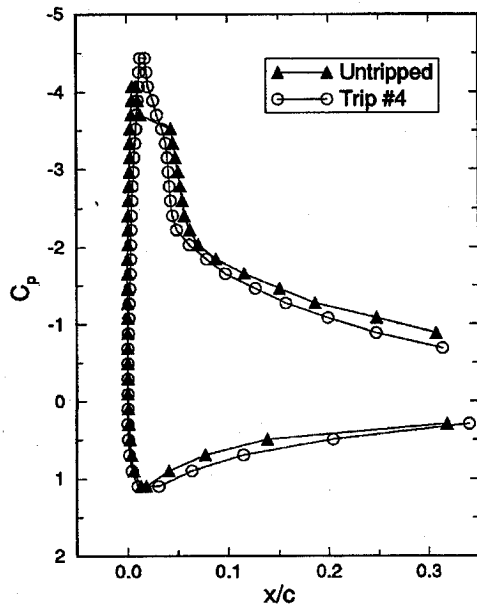

Fig. 6a Surface pressure distribution for untripped and tripped flows; $M = 0.3, k = 0.05$, and $\alpha = 10.65$ deg.
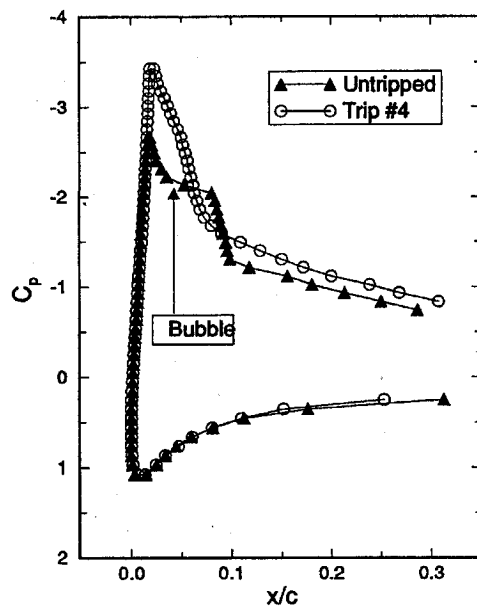

Fig. 6b Surface pressure distribution for untripped and tripped flows; $M = 0.45, k = 0.05$, and $\alpha = 7.97$ deg.

4 shows a higher peak of $C_p = -4.5$ and a gradual fall from the peak. This is consistent with the observations made while discussing Figs. 2 and 3 and with those of Ref. 12. Interestingly, the suction peak shifts slightly downstream when a trip is present, an indication that the outer potential flow is somewhat modified, even though the trip is physically very small. The most dramatic differences are seen between the leading edge and $x/c = 0.1$. Figure 6b is drawn for $M = 0.45$ and $k = 0.05$ at $\alpha = 7.95$ deg. Once again, the presence of the bubble is clearly seen for the untripped flow, and it is absent in the case of the airfoil with trip 4 on it. The larger differences in this higher Mach number flow imply that the viscous/inviscid interactions are considerably affected by the presence of the bubble, reducing its ability to generate higher levels of suction and, thus, dynamic lift.

3. Role of Adverse Pressure Gradient

Separation in both steady and unsteady flows is influenced by the state of the boundary layer and the magnitude of the adverse pressure gradient to which the boundary layer is subjected. To study the flow in greater detail, the adverse pressure gradients for each flow condition were determined by fitting a curve to the measured pressure distributions and obtaining an average pressure gradient over several points. (See Wilder et al.[12] for full details of the procedure.) It should be noted that any method of adverse pressure gradient determination inherently yields noisy data with large uncertainty, since numerical differentiation is involved. Furthermore, it is difficult to precisely detect the origin of the fringes on the airfoil surface due to the presence of the trip itself and the locally high fringe density. Thus, small changes in the streamwise location of the fringes could produce large differences in the pressure gradient, despite the care taken during the process. However, this process, although subjective, is internally consistent, and hence the results are useful.

The nondimensionalized adverse pressure gradient is plotted against angle of attack for the untripped airfoil and for the trip 4 flow at $M = 0.3$. Similar data are available for the other trip flows as well. Since trip 4 was found to be the most satisfactory, the comparison of only the results for this trip with that of the untripped airfoil flow are presented. For the steady flow data shown in Fig. 7a,
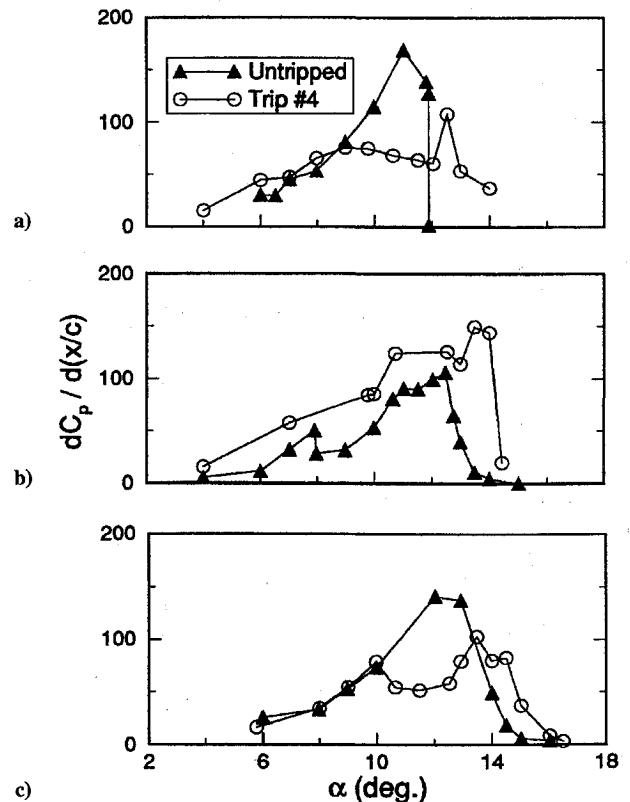

Fig. 7 Leading-edge adverse pressure gradient development, $M = 0.3$: a) $k = 0$, b) $k = 0.05$, and c) $k = 0.1$.

a laminar separation first occurs at $\alpha = 6$ deg when the local adverse pressure gradient is about 30. The flow reattaches by natural transition and static stall develops at $\alpha = 12$ deg when the pressure gradient reaches a value of about 170. With trip 4 on the airfoil, static stall occurs when the pressure gradient becomes about 125, somewhat below the value for the untripped airfoil case. In the untripped unsteady flow at $k = 0.05$, Fig. 7b, laminar separation occurs at around $\alpha = 8$ deg and dynamic stall occurs at $\alpha = 12.5$ deg. The trip 4 flow appears to sustain higher adverse pressure gradients throughout the range of angles of attack considered and dynamic stall eventually sets in when the pressure gradient value is about 150 at $\alpha = 13.5$ deg. At $k = 0.1$, the results in Fig. 7c show a trend similar to that observed in Fig. 7a; the pressure gradient at laminar separation is about 40 and dynamic stall pressure gradient is about 140 for the untripped airfoil flow. For the trip 4 flow, the pressure gradient at stall is about 110 and a definite stall delay is observed. Although at first the untripped airfoil may appear to be better in withstanding higher pressure gradients than the tripped airfoil, it should be noted that the untripped airfoil experienced laminar separation at a very low pressure gradient (of around 30–40) in laminar flow. The resulting bubble due to transition occurring naturally altered the overall pressure distribution. The reattachment in the back end of the bubble also resulted in a different state of turbulence for this case. Thus, it appears that the formation of the bubble may, in fact, have a beneficial effect and is fortuitous to the flow. The drag introduced by the placement of any trip increases the momentum thickness (Preston[9]) and reduces the energy available to overcome the adverse pressure gradient, possibly resulting in separation at lower values of the pressure gradient. In the comparison of the trips, it was found that although the separation pressure gradient was a little lower than that for the untripped flow, trip 4 seems to be the best in simulating higher Reynolds number, since the most improvement in suction levels and, hence, lift was achieved with it. This analysis demonstrates that when selecting a proper trip for the purpose, in the absence of other information such as turbulence and wall shear data, the elimination of the bubble and evaluation of the pressure gradient could be used to assess the effectiveness of the trips. The differences between even similar roughness trips (for example, trips 4 and 5) demonstrate that the state of turbulence is a major factor in providing the boundary layer the ability to overcome the forces causing unsteady flow separation.

4. Global Pressure Distributions

Figures 8a and 8b present the global pressure data obtained by fringe tracing at $\alpha = 14$ deg for $k = 0.05$ and $M = 0.3$ for the untripped airfoil and for trip 4 corresponding to the interferograms in Fig. 3. The results are a quantification of the statements made in Sec. III.A. In addition to the differences in the peak value of the suction pressure coefficient (-3.89 for untripped and -5.9 for trip 4) the entire flowfield is very different. This can be seen by following the highlighted lines in the figures. As stated earlier, these differences can be attributed to the different state of turbulence in the initial or early turbulent boundary layer in the two cases.

Figure 9 compares the pressure fields at $\alpha = 10$ deg for $M = 0.45$ and $k = 0.05$ for the cases when the interferograms showed multiple shocks. The long sequence of multiple shocks (shown by dotted lines nearly normal to the airfoil upper surface) characteristic of laminar flow untripped airfoil dynamic stall[15] was not found for the trip 4 flow. Although a closer examination of Fig. 9b reveals two shocks (discontinuities in the fringe contours), they do not appear to be strong despite the larger Mach number ($C_p = -3.84$) closer to the airfoil. Figure 9c clearly shows that the flow has not fully transitioned with trip 5, since the fringe pattern compares reasonably with that of the untripped airfoil flow. The supersonic region for the untripped airfoil is much flatter than that for the trip 4 flow. The isentropic flow assumptions used limit quantifying the flow details locally between the shocks, but it is clear that, despite the larger suction levels in the case of trip 4 flow, the shocks seen in the supersonic flow region have not induced flow separation. This flow behavior indicates that the flow is more akin to turbulent flow and is similar to the turbulent flow dynamic stall computational results of Visbal[16] and Ekaterinaris.[17] These results affirm that the state of
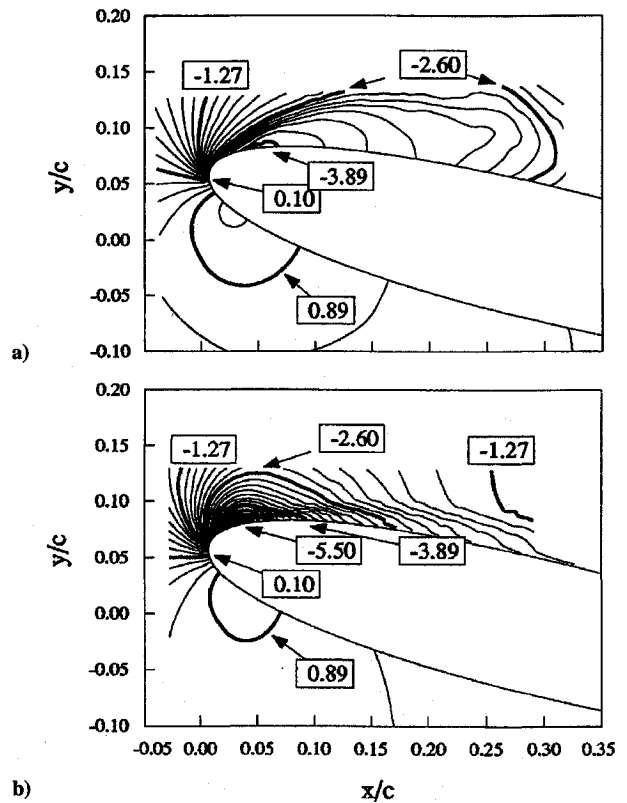

Fig. 8 Global pressure coefficient distributions, $M = 0.3$, $k = 0.05$, and $\alpha = 13.99$ deg: a) untripped and b) trip 4.
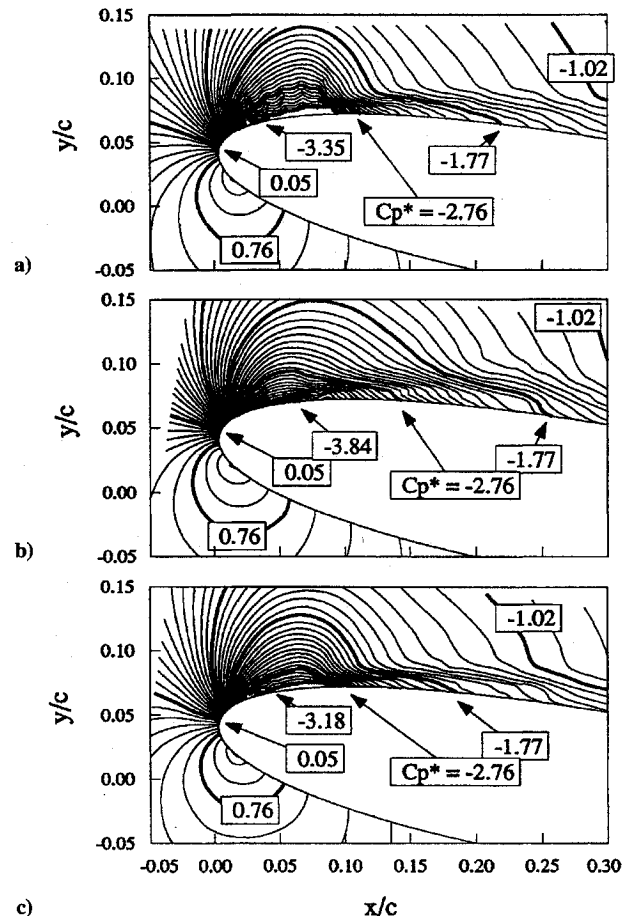

Fig. 9 Global pressure coefficient distributions, $M = 0.45$, $k = 0.05$, and $\alpha = 10.00$ deg: a) untripped, b) trip 4, and c) trip 5.

the turbulence in the turbulent boundary layer plays a very definite role in affecting the dynamic stall process.

C. Freestream Turbulence and Scale Effects on Results

It is well known that wind-tunnel turbulence significantly influences the transition process. Steady flow studies on a NACA 0015 airfoil by Hoffman[18] at $Re = 2.5 \times 10^5$ where laminar/transitional effects are important have shown dramatic increases in the maximum lift coefficient, accompanied by delay of stall, with an increase in freestream turbulence. Similarly, in unsteady pitching airfoil studies in a water tunnel with a freestream turbulence of 0.8% at $Re = 2.2 \times 10^5$ Conger and Ramaprian[19] measured a delay of stall and a suction peak of -17, a value comparable to that obtained in measurements at $Re = 2 \times 10^6$ for incompressible Mach numbers.

Scale effects originate in wind-tunnel tests due to a failure to achieve full-scale Reynolds number and full-scale transition position.[20] In high-incidence model testing, as in dynamic stall studies, the effects appear as a change in the boundary-layer thickness at the separation point due to differences in the transition point location between the high and low Reynolds number flows, as well as a change in the effective Reynolds number due to freestream turbulence. This affects the overall airfoil circulation and, thus, the pressure distribution over the airfoil surfaces. Failure to achieve identical transition location can occur even if the wind-tunnel model and flight vehicle Reynolds numbers are the same. This is because premature transition can be caused in wind-tunnel tests due to roughness, freestream flow unsteadiness, and turbulence. Lorber et al.[21] address the difficulties associated with model rotor testing and extrapolating the data to full-scale testing where complex interactions between rotor wake turbulence and flow over the blade are major issues in addition to scale effects. Carr and Chandrasekhara discuss some of these aspects in greater detail in a recent review article.[22]

The present test results were obtained in a very low turbulence environment. Thus, the effects of freestream turbulence are at a minimum here. Mabey[20] notes that failure to fix transition at an appropriate point on the wind tunnel model is probably more serious than failure to reproduce the correct Reynolds number. Hence, the approach followed in the present tests was to fix the transition point to remove the large variability otherwise introduced in the results by the rapid movement of the transition point as the airfoil is oscillated through a large angle-of-attack range. As mentioned in Sec. I, earlier model rotor scale tests in the CDSF showed that airfoil compressible dynamic stall originated during the bursting of a laminar separation bubble on the airfoil. By carefully tripping the airfoil at a predetermined location, this bubble was removed and thus the experiment provided results that are more relevant to higher Reynolds number flow conditions.

IV. Conclusions

1) The challenging problem of tripping a leading-edge-stalling airfoil under compressible dynamic stall flow conditions was addressed.

2) The criteria for successful tripping were established as the elimination of the laminar separation bubble that otherwise forms, delay of dynamic stall onset angle, and production of larger suction peaks at corresponding angles of attack when compared with an untripped airfoil dynamic stall flow.

3) Five different trips were tested. The results showed that the dynamic stall flow was extremely sensitive to the trip used and hence to the state of turbulence in the flow immediately downstream of the trip.

4) The conventional recommendations for tripping an airfoil to achieve results equivalent to a higher Reynolds number were found not to be applicable in this unsteady leading-edge-stalling flow.

5) The optimum trip was determined to consist of a distributed roughness whose height was comparable to (but less than) the boundary-layer thickness in the adverse pressure gradient region and upstream of the point where the dynamic stall vortex forms over the untripped airfoil. Only one of the trips tested (trip 4) was found to work over the wide range of flow conditions of interest.

6) The large variability in the details of the dynamic stall process of an untripped airfoil was removed by fixing the transition point.

The data thus generated are believed to be useful in validating compressible dynamic stall flow computations.

References

[1]McCroskey, W. J., McAlister, K. W., Carr, L. W., Pucci, S. L., Lambert, O., and Indergrand, R. F., "Dynamic Stall on Advanced Airfoil Sections," *Journal of American Helicopter Society*, Vol. 26, No. 3, 1985, pp. 40–50.

[2]Lorber, P. F., and Carta, F. O., "Unsteady Stall Penetration Experiments at High Reynolds Number," Air Force Office of Scientific Research, AFOSR-TR-87-1202, East Hartford, CT, April 1987.

[3]Chandrasekhara, M. S., and Carr, L. W., "Flow Visualization Studies of the Mach Number Effects on the Dynamic Stall of an Oscillating Airfoil," *Journal of Aircraft*, Vol. 27, No. 6, 1990, pp. 516–522.

[4]Chandrasekhara, M. S., Ahmed, S., and Carr, L. W., "Schlieren Studies of Compressibility Effects on Dynamic Stall of Airfoils in Transient Pitching Motion," *Journal of Aircraft*, Vol. 30, No. 2, 1993, pp. 213–220.

[5]Gostelow, J. P., Blunden, A. R., and Walker, G. J., "Effects of Free-Stream Turbulence and Adverse Pressure Gradients on Boundary Layer Transition," American Society of Mechanical Engineers, ASME Paper 92-GT-380, New York, June 1992.

[6]Jones, R., and Williams, D. H., "The Effect of Surface Roughness on the Characteristics of the Aerofoils N.A.C.A. 0012 and R.A.F. 34," National Physical Lab., Reports and Memoranda No. 1708, London, Feb. 1936.

[7]Nakamura, Y., and Tomonari, Y., "The Effects of Roughness on the Flow Past Circular Cylinders at High Reynolds Numbers," *Journal of Fluid Mechanics*, Vol. 123, Oct. 1982, pp. 363–378.

[8]Pope, A., and Goin, K. L., "Calibration and Use of Nearsonic and Transonic Tunnels," *High Speed Wind Tunnel Testing*, Kraeger, New York, 1978, pp. 305–348.

[9]Preston, J. H., "The Minimum Reynolds Number for a Turbulent Boundary Layer and the Selection of a Transition Device," *Journal of Fluid Mechanics*, No. 3, Pt. 4, 1958, pp. 373–384.

[10]Carr, L. W., and Chandrasekhara, M. S., "Design and Development of a Compressible Dynamic Stall Facility," *Journal of Aircraft*, Vol. 29, No. 3, 1992, pp. 314–318.

[11]Davis, S. S., "Measurement of Discrete Vortex Noise in a Closed Throat Wind Tunnel," AIAA Paper 75-488, March 1975.

[12]Wilder, M. C., Chandrasekhara, M. S., and Carr, L.W., "Transition Effects on Compressible Dynamic Stall of Transiently Pitching Airfoils," AIAA Paper 93-2978, July 1993.

[13]Brock, N. J., Chandrasekhara, M. S., and Carr, L. W., "A Real Time Interferometry System for Unsteady Flow Measurements," *ICIASF'91 RECORD*, Inst. of Electrical and Electronics Engineers, IEEE Publication 91-CH3028-8, pp. 423–430.

[14]Carr, L. W., Chandrasekhara, M. S., and Brock, N. J., "Quantitative Study of Compressible Flow on an Oscillating Airfoil," *Journal of Aircraft*, Vol. 31, No. 4, 1994, pp. 892–898.

[15]Chandrasekhara, M. S., Carr, L. W., and Wilder, M. C., "Interferometric Investigations of Compressible Dynamic Stall over a Transiently Pitching Airfoil," *AIAA Journal*, Vol. 32, No. 3, 1994, pp. 586–593.

[16]Visbal, M. R., "Effect of Compressibility on Dynamic Stall of a Pitching Airfoil," AIAA Paper 88-0132, Jan. 1988.

[17]Ekaterinaris, J. A., "Compressible Studies of Dynamic Stall," AIAA Paper 89-0024, Jan. 1989.

[18]Hoffman, J. A., "Effects of Freestream Turbulence on the Performance Characteristics of an Airfoil," *AIAA Journal*, Vol. 29, No. 9, 1991, pp. 1353, 1354.

[19]Conger, R. N., and Ramaprian, B. R., "Pressure Measurements on a Pitching Airfoil in a Water Channel," Dept. of Mechanical and Materials Engineering, Rept. MME-TF-92-3, Washington State Univ., Pullman, WA, May 1992.

[20]Mabey, D. G., "A Review of Scale Effects in Unsteady Aerodynamics," *Progress in Aerospace Sciences*, Vol. 28, No. 4, 1991, pp. 273–321.

[21]Lorber, P. F., Stauter, R. C., Haas, R. J., Anderson, T. J., Torok, M. S., and Kohlhepp, F. W., "Techniques for Comprehensive Measurement of Model Rotor Aerodynamics," *Proceedings of the American Helicopter Society Forum 50*, Washington, DC, May 1994.

[22]Carr, L. W., and Chandrasekhara, M. S., "An Assessment of the Impact of Compressibility on Dynamic Stall," AIAA Paper 95-0779, Jan. 1995.